JOURNAL OF ENVIRONMENTAL SCIENCES 52 (2017) 293–304

Available online at www.sciencedirect.com

ScienceDirect

www.elsevier.com/locate/jes

JES JOURNAL OF ENVIRONMENTAL SCIENCES

www.jesc.ac.cn

Chemical characterization and source apportionment of atmospheric submicron particles on the western coast of Taiwan Strait, China

Liming Cao[1], *Qiao Zhu*[1], *Xiaofeng Huang*[1], *Junjun Deng*[2], *Jinsheng Chen*[2], *Youwei Hong*[2], *Lingling Xu*[2], *Lingyan He*[1,*]

1. *Key Laboratory for Urban Habitat Environmental Science and Technology, School of Environment and Energy, Peking University Shenzhen Graduate School, Shenzhen 518055, China*

2. *Center for Excellence in Urban Atmospheric Environment, Institute of Urban Environment, Chinese Academy of Sciences, Xiamen 361021, China*

ARTICLE INFO

Article history:
Received 29 May 2016
Revised 30 August 2016
Accepted 14 September 2016
Available online 15 November 2016

Keywords:
Submicron particle
Chemical characterization
Organic aerosol
Source apportionment

ABSTRACT

Taiwan Strait is a special channel for subtropical East Asian Monsoon and its western coast is an important economic zone in China. In this study, a suburban site in the city of Xiamen on the western coast of Taiwan Strait was selected for fine aerosol study to improve the understanding of air pollution sources in this region. An Aerodyne high-resolution time-of-flight aerosol mass spectrometer (HR-ToF-AMS) and an Aethalometer were deployed to measure fine aerosol composition with a time resolution of 5 min from May 1 to 18, 2015. The average mass concentration of PM1 was 46.2 ± 26.3 μg/m3 for the entire campaign. Organics (28.3%), sulfate (24.9%), and nitrate (20.6%) were the major components in the fine particles, followed by ammonium, black carbon (BC), and chloride. Evolution of nitrate concentration and size distribution indicated that local NOx emissions played a key role in high fine particle pollution in Xiamen. In addition, organic nitrate was found to account for 9.0%–13.8% of the total measured nitrate. Positive Matrix Factorization (PMF) conducted with high-resolution organic mass spectra dataset differentiated the organic aerosol into three components, including a hydrocarbon-like organic aerosol (HOA) and two oxygenated organic aerosols (SV-OOA and LV-OOA), which on average accounted for 27.6%, 28.8%, and 43.6% of the total organic mass, respectively. The relationship between the mass concentration of submicron particle species and wind further confirmed that all major fine particle species were influenced by both strong local emissions in the southeastern area of Xiamen and regional transport through the Taiwan Strait.

Introduction

Submicron particles, whether natural or anthropogenic, originate from emissions of primary particulate matter and secondary particulate matter from gaseous precursors (IPCC , 2013). Submicron particles are crucial air pollutants in the urban environment and they have important effects on human health, visibility and climate change, the adverse health effects are of special concern in metropolitans (Baklanov et al., 2016). Organics contribute a large fraction to the submicron particles and are poorly understood (Zhang et al., 2007). Apportioning organic species into their sources and components correctly is a critical

* *Corresponding author*. E-mail: hely@pku.edu.cn (Lingyan He).

http://dx.doi.org/10.1016/j.jes.2016.09.018
1001-0742/

step towards enabling efficient control strategies and model representations (Ulbrich et al., 2009). Submicron particles are a complicated mixture of various species, it is essential to have a deep understanding of the chemical identification and source apportionment.

Although many studies focused on submicron particles in atmosphere were carried out in Yangtze River Delta region, Pearl River Delta region and Beijing–Tianjin–Hebei region (Feng et al., 2009; Huang et al., 2012, 2013, 2014; He et al., 2011; Hu et al., 2016), there are few studies about the Taiwan Strait. Both the west and east sides of the Taiwan Strait are mountainous and coastal terrain that make it a special channel for the airmass transportation in eastern China. The area around the Taiwan Strait is mainly influenced by subtropical East Asian Monsoons and the special climatic conditions such as sea-land breeze and high RH (Deng et al., 2014). The west side of the Taiwan Strait is an important economic zone in China like Pearl River Delta (PRD) and Yangtze River Delta (YRD). There are many important industrial and densely populated areas on both the west and east side of the Taiwan Strait, which can emit large amount of particulate pollutants transported through the Taiwan Strait along with the airflow. Xiamen (24°36′N, 118°03′E) is one of the most important metropolitan in the west side of the Taiwan Strait economic zone with an area of 1573.16 km^2 and a population of 3.81 million. Like many other cities in China, Xiamen also suffers a big problem of air pollution with the rapid development of economy and urbanization. The industrial plants in Xiamen, including coal-fired power plants, ceramic plants, porcelain products and textile industry, can be the potential emission sources for air pollution. So the submicron particle pollution in Xiamen, to the west side of the Taiwan Strait, is not only under the influence of local emissions, but also obviously affected by regional sources transported along the coast.

Although some studies have been taken on the properties of submicron particles in Xiamen, but the chemical characteristics and source apportionment was rarely studied. The result in Zhang et al. (2012) show an annual average concentration of $PM_{2.5}$ of 86.16 $\mu g/m^3$ during June 2009 to May 2010, focusing on a long lasting period. Zhang et al. (2013) showed that the average mass concentration of $PM_{2.5}$ of the period before, during and after hazy from Dec. 25, 2010 to Jan. 1, 2011 were 88.80 ± 19.97, 135.41 ± 36.20 and 96.35 ± 36.26 $\mu g/m^3$, respectively, focusing on the chemical compositions, light extinction and metropology in Xiamen. Some other previous studies showed that organic matter and sulfate were the most abundant components of fine particles in Xiamen, followed by ammonium and nitrate (Wu, 2015; Yan et al., 2015).

High-resolution time-of-flight aerosol mass spectrometer (HR-ToF-AMS, Aerodyne, US) is a very useful instrument to measure the chemical composition and size distribution of non-refractory species. This paper reports the size resolved chemical characterization measured by an HR-ToF-AMS, coupled with an Aethalometer to measure black carbon aerosol, and the results of factor analysis for organic aerosol source apportionment with the high-resolution of the organic mass spectra in the air in Xiamen in May 2015, aims to have a further understanding of the chemical composition and variation of submicron particles in Taiwan Strait region.

1. Experimental methods

1.1. Sampling site description

The sampling site was located in the Institute of Urban Environment, Chinese Academy of Sciences (IUE, CAS) in the Jimei District, and was a suburban site close to the Xinglin Bay. Since this site was located roughly at the geometric center of the Xiamen territory and in the downwind area of urban Xiamen during the sampling period, it could serve as a good receptor site of various pollutant sources in this region, reflecting not only urban emissions but also industrial emissions. The campus and its surroundings were mostly covered by subtropical plants. Two local roads are about 100 m far away to the northwest and northeast, respectively. The field campaign was conducted from 1 May to 18 May 2015. The average ambient temperature was 24.3 ± 2.9°C. In winter, the air quality in Xiamen can be greatly influenced by the air mass transported from the more polluted northern inland, so the local emissions in this region cannot be obviously observed. While in summer, the air quality is quite good due to the abundant precipitation and the clean air mass from the sea, which makes summer not an ideal choice for air pollution research. Therefore, the spring time, as a transition season, was selected for this study.

1.2. HR-ToF-AMS measurement and data process

An Aerodyne High-Resolution Time-of-Flight Aerosol Mass Spectrometer (referred as AMS) was deployed in an air monitoring station in the campus of IUE, CAS with a $PM_{2.5}$ cyclone inlet set up on the roof of the station to remove coarse particles and lead the airflow into the room with a flow rate of 10 L/min. The detailed principles of the operation of AMS were described in previous publications (DeCarlo et al., 2006; Canagaratna et al., 2007). During the campaign, the AMS was operated in a cycle of 2 ion optical modes (V and W), including 2 min V-mode to obtain the UMR mass concentration and size distribution of the non-refractory species (organics, SO_4^{2-}, NO_3^-, NH_4^+ and Cl^-); 2 min W-mode to obtain high-resolution mass spectra of organics. The inlet flow rate calibration, ionization efficiency (IE) and particle size calibration was conducted at the beginning and the end of the campaign with the method described in previous publications (Jayne et al., 2000; Jimenez et al., 2003; Drewnick et al., 2005). The detection limits of AMS for different species were determined by filtered particle-free ambient air and defined as three times the standard deviations of the corresponding species (Zhang et al., 2005a; DeCarlo et al., 2006; Sun et al., 2009). The detection limits of organics, sulfate, nitrate, ammonium and chloride for 2 min V-mode averaging during the campaign were 0.244 $\mu g/m^3$, 0.064 $\mu g/m^3$, 0.05 $\mu g/m^3$, 0.231 $\mu g/m^3$ and 0.042 $\mu g/m^3$, respectively. Refractory black carbon (BC), which cannot be detected by AMS, was measured simultaneously by an Aethalometer (AE-31, Magee, US) coupled with a $PM_{2.5}$ cyclone with a time resolution of 5 min. The wavelength of 880 nm was used for BC mass concentration calculation in the Aethalometer data processing.

Data analysis was performed with software packages SQUIRREL version 1.57 and PIKA version 1.16 (http://cires.

colorado.edu/jimenez-group/ToFAMSResources/ToFSoftware/index.html) following the method shown in DeCarlo et al. (2006). The mass concentration should be corrected with collection efficiency (CE) due to the loss of particles when transmitting through the aerodynamic lens and bouncing at the vaporizer. The potential influence of RH on particle collection efficiency (CE) at the vaporizer was eliminated since a nafion dryer was placed upstream of the AMS to keep the relative humidity of the particles less than 30% (Matthew et al., 2008). Middlebrook et al. (2012) revealed that CE can be affected by many factors, including the composition, acidity, ammonium nitrate fraction, organic fraction of the particles. The calculated composition-dependent CE based on Middlebrook et al. (2012) was applied to the data. The default values of relative ionization efficiency (RIE) values were used in this study (1.2 for sulfate, 1.1 for nitrate, 1.3 for chloride, 1.4 for organics and 4.0 for ammonium) (Jimenez et al., 2003).

1.3. Estimation of organic nitrates

Organic nitrates (R-ONO_2) are formed through reactions of NO with organic peroxy radicals during the day and through NO_3 radical-initiated reactions of alkenes in the nighttime (Roberts, 1990; Atkinson, 1997; Atkinson and Arey, 2003; Gong et al., 2005; Ng et al., 2008; Fry et al., 2009; Lim and Ziemann, 2009; Matsunaga and Ziemann, 2009). Oxidation of the major atmospheric VOCs leads to a variety of organic nitrate products are mostly multifunctional (Day et al., 2010). Nitrate measured by HR-ToF-AMS is the total nitrate functionality both from inorganic nitrates and organic nitrates. The direct way to measure organic nitrates is not available now. Several methods to calculate organic nitrates with the HR-ToF-AMS were presented in the works by Farmer et al. (2010), Xu et al. (2015) as follows: (1) NO_x^+ ratio; (2) HNO_3/NO_x ratios; (3) $C_xH_yO_zN^+$ fragments; (4) ammonium balance; (5) difference between total and inorganic NO_3^-; (6) PMF analysis.

NO_x^+ ratio method is based on the NO^+/NO_2^+ ratio in the AMS mass spectra and verified to be more reliable (Farmer et al., 2010; Xu et al., 2015). The observed NO^+/NO_2^+ ratio is different for organic nitrates and NH_4NO_3. The NO_x^+ ratio is approximately 10 from the unit mass resolution *m*/*z* of 30 and *m*/*z* of 46 of aerosols derived from the reaction of NO_3 + beta-pinene, 10–15 for aerosols derived from NO_3 + monoterpene, about 5 for NO_3 + isoprene, which were found to be much larger than that of NH_4NO_3 (Fry et al., 2009; Bruns et al., 2010; Farmer et al., 2010) (Table 1). As NO_x^+ ratios are different for organic nitrates and NH_4NO_3, Farmer et al. (2010) and Xu et al. (2015) presented the method to calculate organic nitrates by Eqs. (1)–(4):

$$x = \frac{(R_{obs} - R_{AN})(1 + R_{ON})}{(R_{ON} - R_{AN})(1 + R_{obs})} \quad (1)$$

$$NO_{2,org} = \frac{NO_{2,obs} \times (R_{obs} - R_{AN})}{(R_{ON} - R_{AN})} \quad (2)$$

$$NO_{org} = R_{ON} \times NO_{2,org} \quad (3)$$

$$NO_{3,org} = NO_{2,org} + NO_{org} \quad (4)$$

The fraction of organic nitrates group in the total nitrate signal (*x*) can be estimated by Eq. (1). R_{obs} is the NO_x^+ ratio from observation, R_{AN} is the NO_x^+ ratio from pure ammonium nitrate, R_{ON} is the NO_x^+ ratio from organic nitrates, NO_{org} and $NO_{2,org}$ is the concentration of fragments NO^+ and NO_2^+ in organic nitrates, $NO_{3,org}$ is the concentration of organic nitrates. The R_{AN} was determined from the ionization efficiency (IE) calibration using 300 nm ammonium nitrate particles (Xu et al., 2015). R_{ON} is the NO_x^+ ratio for organic nitrates, but the time series of R_{ON} cannot be applied in Eqs. ((1)–(2)) since it is unavailable to measure every ambient organic nitrate species required by time-dependent R_{ON}. R_{AN} and R_{ON} are reported vary between different instruments (Fry et al., 2009; Farmer et al., 2010; Rollins et al., 2010; Bruns et al., 2010; Boyd et al., 2015). R_{AN} in this study varied between 2.88–3.18, and the mean value (3.02 ± 0.09) was used to calculate the range of R_{ON}.

1.4. PMF analysis method

Positive matrix factorization (PMF) (Paatero and Tapper, 1994) analysis was used to identify major organic component with the data and error matrix generated with the fragmentation waves selected in PIKA. High-resolution organic mass spectra data collected by AMS has been analyzed by PMF evaluation tool developed by Ulbrich et al. (2009) for many previous field campaign (Huang et al., 2012, 2013; Hu et al., 2016). The error matrix was calculated as the sum of Poisson ion-counting error and electronic error for the fragments (Allan et al., 2003; Ulbrich et al., 2009). Signal to noise ratio (SNR) was a standard for preparing the data matrix: ions with 0.2 < SNR < 2 were regarded as weak ions and downweighted by a factor of 2; while ions with SNR < 0.2 were classified into bad ions and removed from the analysis (Paatero and Hopke, 2003). Because of the relationship with CO_2^+, the ions of O^+, HO^+, H_2O^+, and CO^+ were downweighted as the *m*/*z* of 44 related species from the data and error matrices to avoid over weighting of CO_2^+ (Ulbrich et al., 2009). The rotational ambiguity was tested by the change of parameter FPEAK and the robustness of PMF solutions was evaluated by changing parameter seed. Huang et al. (2010) and He et al. (2011) presented the principles of the selection of the optimal solution in detail: $Q/Q_{expected}$ ratio (Q and $Q_{expected}$ refer to the actual and ideal sum of the squares of PMF least square fitted scaled residuals), the characteristic of different mass spectrums, the time series and correlation with external tracers of each factor.

PMF analysis of this campaign was conducted based on the high-resolution mass spectrums for 1 to 8 factors with FPEAK varying from −1 to 1 (seed = 0) in increment of 0.1 and seed varying from 0 to 250 in step of 10 (FPEAK = 0) in this campaign. As discussed in Table 2, the three factors, FPEAK = 0, seed = 0 solution was chosen as the optimal solution for this study, including a hydrocarbon-like organic aerosol (HOA), a

Table 1 – Values of R_{AN}/R_{ON} and R_{ON} referred to previous studies.

Species	R_{ON}/R_{AN}	R_{ON}	Reference
Six organic nitrate standards	2.25 ± 0.35	5.98 ± 0.17	Farmer et al. (2010)
Isoprene	2.08	5.53 ± 0.06	Bruns et al. (2010)
Beta-pinene	3.99 ± 0.25	10.61 ± 0.09	Boyd et al. (2015)
Aromatic VOCs	2.49	6.62 ± 0.06	Sato et al. (2010)

semi-volatile oxygenated organic aerosol (SV-OOA) and a less-volatile oxygenated organic aerosol (LV-OOA).

2. Results and discussion

2.1. PM_1 chemical compositions

Fig. 1a shows the time series of the mass concentration of all the species measured by AMS and Aethalometer during the campaign in Xiamen. The hazy periods were relatively short because of the frequent rain and strong winds during the campaign. The mean PM_1 (the sum of species measured by AMS and BC from Aethalometer) mass concentration was 46.2 ± 26.3 μg/m^3, ranging in 2.7–164.4 μg/m^3. The particle mass concentration measured with a collocated Scanning Mobility Particle Sizer (SMPS, TSI) by assuming spherical particles was calculated from the number size distribution between 15 and 600 nm in Stocks diameter (equal to 22–900 nm in vacuum aerodynamic diameter). The mean value of the PM_1 density calculated with Eq. (5) was 1.54 ± 0.04 g/cm^3, where, ρ is the density of PM_1, M and V are the mass concentration and volume concentration of PM_1, respectively, $[SO_4^{2-}]$, $[NO_3^-]$, $[NH_4^+]$, $[Cl^-]$, [Org] and [BC] are the mass concentration of sulfate, nitrate, ammonium, chloride, organics and black carbon, respectively. The linear correlation coefficient (R^2) of PM_1 and SMPS mass concentration calculated with SMPS volume concentration and density from Eq. (5) was 0.88, with a slope of 1.1 (Fig. 1b). The composition-dependent CE of AMS used in this study seems to be reasonable when taking into account the measurement uncertainties of both AMS and SMPS, though there may be possibly a positive bias for the slope of 1.1, which is indicative of underestimation of aerosol density to some extent which may be caused by the uncertainties of calculation or trace metals in PM_1. On average, organics and sulfate were the most abundant PM_1 components, accounted for 28.3% and 24.9% of the PM_1, respectively, followed by nitrate (20.6%), ammonium (16.2%), black carbon (8.9%) and chloride (1.1%) as shown in Fig. 1c.

$$\rho = \frac{M}{V} = M \Big/ \left(\frac{[SO_4^{2-}]}{1.78} + \frac{[NO_3^-]}{1.72} + \frac{[NH_4^+]}{1.75} + \frac{[Cl^-]}{1.55} + \frac{[Org]}{1.2} + \frac{[BC]}{1.7} \right) \quad (5)$$

Fig. 1d shows the relative contributions of different species as a function of the total mass concentration. The relative contribution of organics and ammonium kept a relatively stable fraction of ~29% and ~16%, respectively, the relative contribution of sulfate was decreasing with the increasing of PM_1 mass concentration, while nitrate showed a reverse trend, suggesting that photochemical reactions played an important role in the formation of PM_1 pollutants. The contribution of nitrate showed a significant increasing trend (from ~10% (at mass concentration <30 μg/m^3) to ~28% (at mass concentration >130 μg/m^3)) while that of sulfate showed a decreasing trend (from ~32% (at mass concentration <30 μg/m^3) to ~16% (at mass concentration >130 μg/m^3)) as the increasing of PM_1 mass concentration. This feature can also be figured out in the time series of nitrate and sulfate in Fig. 1a. It can be thus inferred that NO_x emissions contributed largely during heavy polluted period in Xiamen.

2.2. Diurnal cycle of PM_1 species

The mean diurnal variations of different PM_1 species during the campaign in box plots are presented in Fig. 2. The diurnal variations of submicron particles are affected by various factors. The higher planetary boundary layer (PBL) in the daytime is considered to be the crucial factor that led to the decreasing of PM_1 mass concentration, while the sunlight would initiate photochemical formation of secondary species, such as organics, nitrate and sulfate (Zhang et al., 2005b; Salcedo et al., 2006; Hennigan et al., 2008; Zheng et al., 2008; Xiao et al., 2009). The diurnal variations of chloride and black carbon showed a similar peak at about 7:00 a.m. mainly caused by the rush hour traffic emissions in the early morning, it then went down due to the lift of the boundary layer. On the other hand, the diurnal variation of chloride can also be influenced by the ambient temperature due to the semi-volatility of NH_4Cl. Therefore, it was found that the mass concentration of chloride went down more deeply in the daytime because of the rising of the ambient temperature. After the peaks of chloride and BC, the diurnal variation showed a small peak for nitrate and sulfate in sequent at around 8:00 a.m., implying that nitrate and sulfate were secondarily formed after the rush hour traffic emissions. Nitrate, sulfate and organics all showed a slight peak in the afternoon, possibly being a balanced result of secondary formation and PBL dilution. Sulfate kept a relatively stable diurnal trend, which implies that sulfate was mostly from large-scale regional transportation, being a more regional product from the oxidation of SO_2 (Salcedo et al., 2006), so sulfate could be mixed thoroughly and less influenced by the change of PBL. And also, sulfate was a less-volatile species and thus would not evaporate to loss its particulate mass during the daytime when the ambient temperature is increasing. The diurnal variation of ammonium was a combined result of

Table 2 – Diagnostics and description of PMF solutions.

No. of factors	FPEAK	Seed	$Q/Q_{expected}$	Diagnostics and description
1	0	0	2.2	Only one factor, larger residuals at some key *m/z* and time periods
2	0	0	1.6	Factors are too few, only HOA and OOA are identified, the spectra and time series were misted with each other
3	0	0	1.48	Optimum number of factors, HOA, SV-OOA and LV-OOA are identified, and the time series correlated well with tracers
4–8	0	0	1.4–1.3	The factors were split
3	−1 to 1	0	1.47976-1.4865	$Q/Q_{expected}$ lowest at FPEAK of 0
3	0	0–250	1.47979	MS and time series are identical as seed varies from 0 to 250

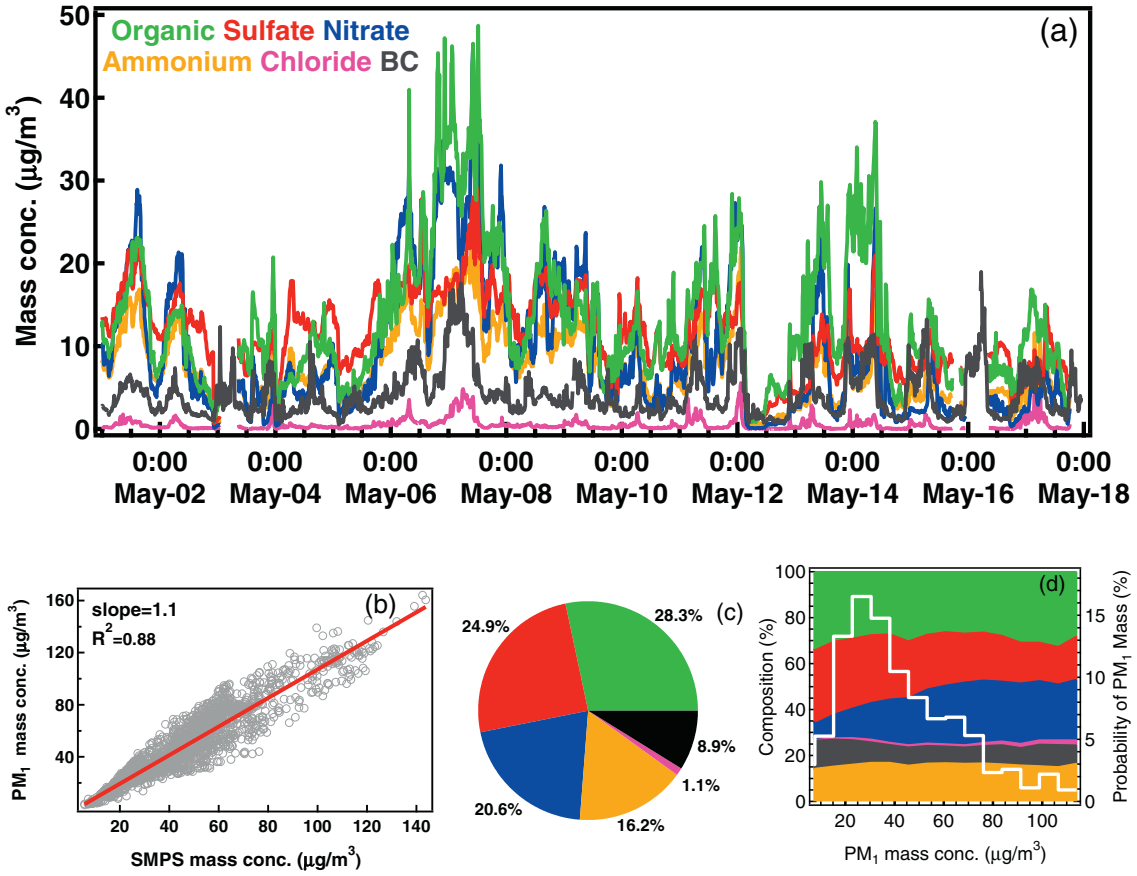

Fig. 1 – (a) Time series and characteristics of PM_1 composition; (b) the correlation between PM_1 mass concentration and SMPS mass concentration; (c) the mass percentage of PM_1 species; (d) the variation of percent composition with PM_1 mass loading in 2015.

particulate $(NH_4)_2SO_4$ and NH_4NO_3. Organics showed a much more complex diurnal variation as the outcome of many different types of organic compounds that emitted by various primary and secondary sources which will be discussed in Section 2.5.

2.3. Size distribution

The average size distribution of all the five species measured by AMS is shown in Fig. 3a, notice that the mass loading of chloride was multiplied by 100 to make it much more comparable with other species within the same scale. All the species were in accumulation modes peaking at 500–600 nm, which is indicative of aged regional aerosol (Allan et al., 2003; Alfarra et al., 2004; Zhang et al., 2005b). The size distribution of organics showed was much broader at smaller size and the integral mean value of the size was at ~400 nm for organics, while it was at ~550–600 nm for all the inorganic species.

The similar average size distribution of the inorganic species indicated that they were likely internally mixed and came from similar gas-to-particle condensation processes. Similar size distribution of the non-refractory species was also observed in urban sites, such as Beijing (Huang et al., 2010) and Shenzhen (He et al., 2011). It is clear that the size distribution of organics was much wider than other species, especially at smaller sizes. And the organics contributed more and more to the total PM_1 mass with the decrease of the size of the particles, which was reasonably due to the fresh organic particles emitted by vehicles from the highways around the site. The gap between sulfate and nitrate was getting wider with the increase of the particle sizes, indicating that more aged larger sulfate particles were transported regionally.

Fig. 3b, c, d shows the relative size distributions of organics, sulfate and nitrate as a function of the mass concentration of organics, sulfate and nitrate, respectively. The relative size distribution was calculated by normalizing the size distribution with the corresponding mass concentration. With the increase of mass concentration, the size distribution of organics and nitrate would get wider, while sulfate peaked at large sizes and the peak was narrowed. The characteristics indicated that organics and nitrate formed locally played an important role and sulfate was mainly dominated by regional transported aerosols during heavy pollution.

2.4. Estimation of organic nitrates

Organic nitrates are important substituents in secondary organic aerosols due to their important effects on nitrogen cycle and ozone production. The nitrate functional group in

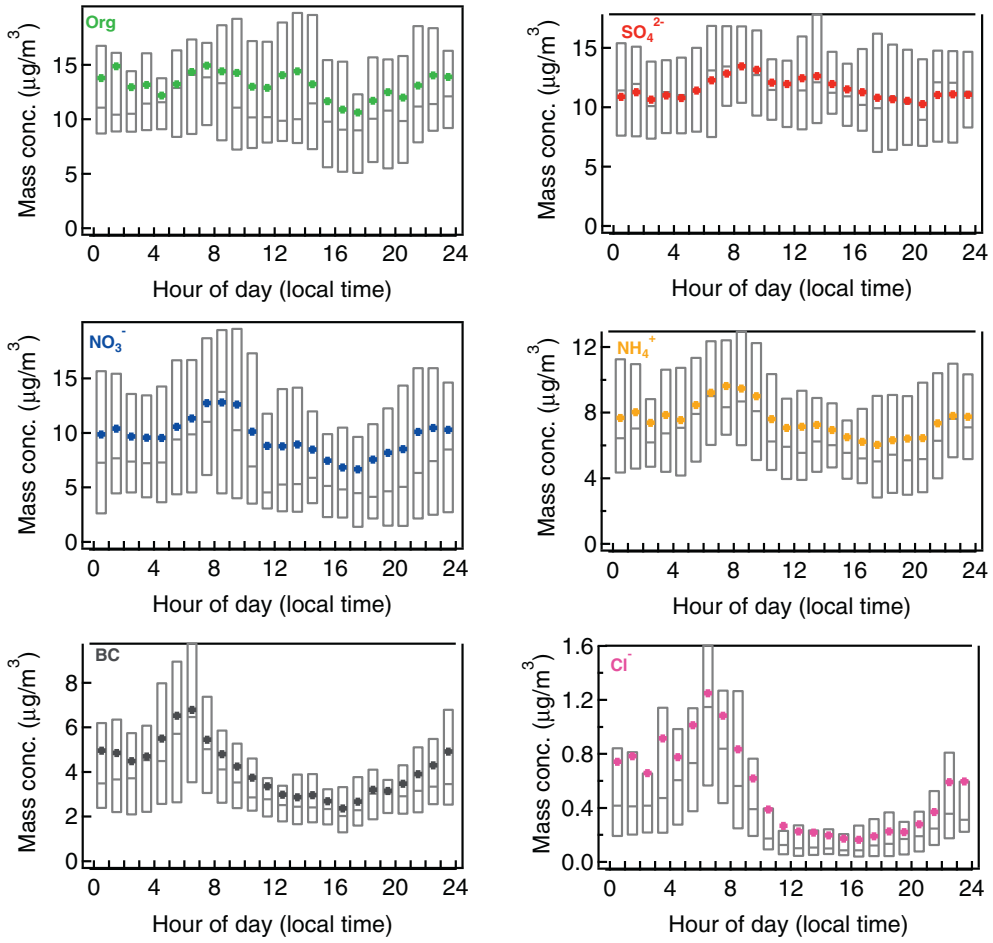

Fig. 2 – Diurnal variation box plots of PM_1 species in Xiamen. The upper and lower boundaries of boxes indicate the 75th and 25th percentile; the lines within the box marks indicate the medians and the cross symbols represent the mean values.

organic nitrates accounts for 5–10% of organics (O'Brien et al., 1975; Mylonas et al., 1991; Laurent and Allen, 2004). Xu et al. (2015) showed that the nitrate functionality from organic nitrates contributes 63%–100% to the total measured nitrates in summer and the contribution of organic nitrates to total OA is 5%–12% in summer, but organic nitrates in the atmosphere are rarely studied in China.

The organic nitrates are calculated by NO_x^+ ratio method with the NO^+/NO_2^+ ratio from the AMS mass spectra as discussed in Section 1.3. The organic nitrates formed from isoprene and beta-pinene was selected as representatives because they can cover a wide range of R_{ON} values as shown in Table 1 and provide a better estimate of organic nitrates. The organic fraction of the organic nitrates molecules was assumed to be 200 g/mol per ONO_2 group by Farmer et al. (2010). The nitrate functionality from organic nitrates to total nitrate ratio was calculated to be 9.0–13.8% in this study, which is quite low compared to the ratio measured in summer in the US reported by Xu et al. (2015). The organic fraction of the organic nitrates may account 21.0–32.5% (2.8–4.3 μg/m^3) of the total organics measured by AMS, which shows that organic nitrates was an significant source for organic aerosol pollution in Xiamen.

2.5. *PMF analysis*

Organics was one of the most important submicron particulate air pollutants in Xiamen, and it was much more complicated than inorganics because of the various emission sources and affected by many factors as discussed above. Positive matrix factorization (PMF) was conducted and analyzed based on the high-resolution mass spectrums measured with HR-ToF-AMS as showed in Section 1.3. Based on all the tests, the three factors, FPEAK = 0, seed = 0 solution was chosen as the optimal solution for this study, including a hydrocarbon-like organic aerosol (HOA), two oxygenated organic aerosol (SV-OOA and LV-OOA). Fig. 4 shows the MS profile of the three components and Fig. 5a–c presents the time series during the campaign. As shown in Fig. 5d, HOA, SV-OOA and LV-OOA on average accounted for 27.6%, 28.8% and 43.6% of the total organic mass, respectively. The organic mass to organic carbon ratio (OM/OC), oxygen to carbon ratio (O/C) and hydrogen to carbon ratio (H/C) were calculated with the Improved Aiken (I-A) method described in Canagaratna et al. (2015), which will be more reasonable than the traditional Ambient Aiken (A-A) method (Aiken et al., 2007, 2008). The Improved-Ambient method elemental analysis was applied to previously published ambient datasets by

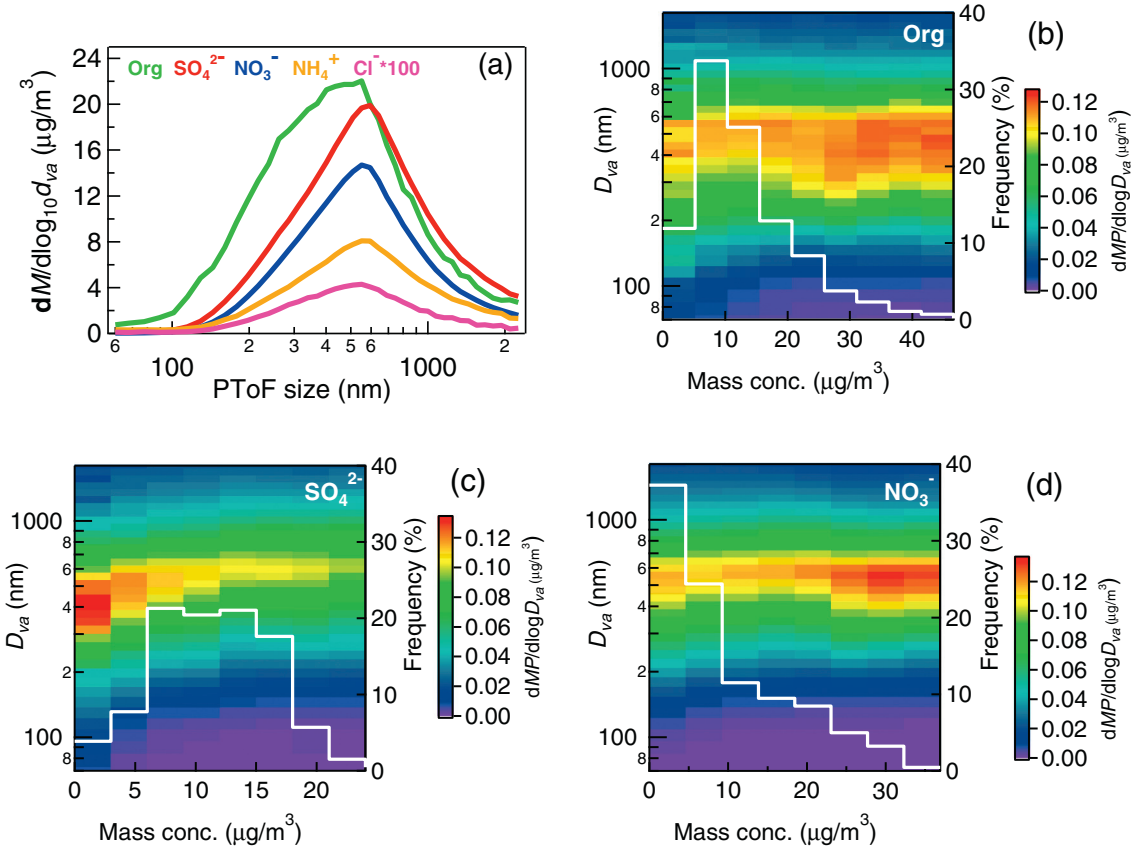

Fig. 3 – (a) Average size distributions of the AMS species; (b–d) the variations of relative size distribution of organics, sulfate, and nitrate with mass concentration. The white lines in Fig. 3b–d stand for the frequencies of the species mass concentration levels occurred during the campaign.

Canagaratna et al. (2015) and showed an increase of the O/C, H/C, OM/OC values of total OA by 27%, 11%, 9% on average, respectively, indicating that the oxygen content of ambient OA is larger than reported by previous AMS measurements. All the elemental ratios in this paper are in I-A method if there is no additional illustration.

The O/C of HOA was 0.26 (0.21 in A-A) in Xiamen campaign, and it is generally low and dominated by the long chain hydrocarbon ion series of $C_nH^+_{2n+1}$ and $C_nH^+_{2n-1}$, which was consistent with the clear hydrocarbon signatures in the spectrum (Canagaratna et al., 2004; Mohr et al., 2009; Ng et al., 2010). As shown in previous factor analyses of AMS ambient aerosol datasets, HOA was mainly attributed to primary fuel combustion sources (Zhang et al., 2007; Lanz et al., 2007; Ulbrich et al., 2009). Since black carbon (BC) can be significantly emitted from fuel combustion and biomass burning, the time series of HOA correlated well with that of BC (R^2 = 0.60). The quite similar diurnal variations of HOA and BC confirming that fuel combustion can be an obvious source for HOA. The HOA in Xiamen had a similar O/C to HOA identified in previous studies in Mexico City

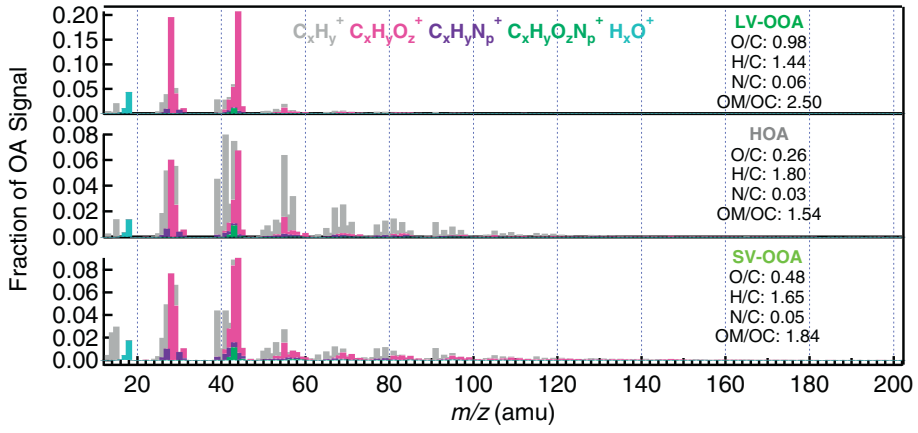

Fig. 4 – MS profiles of the three organic components identified by PMF.

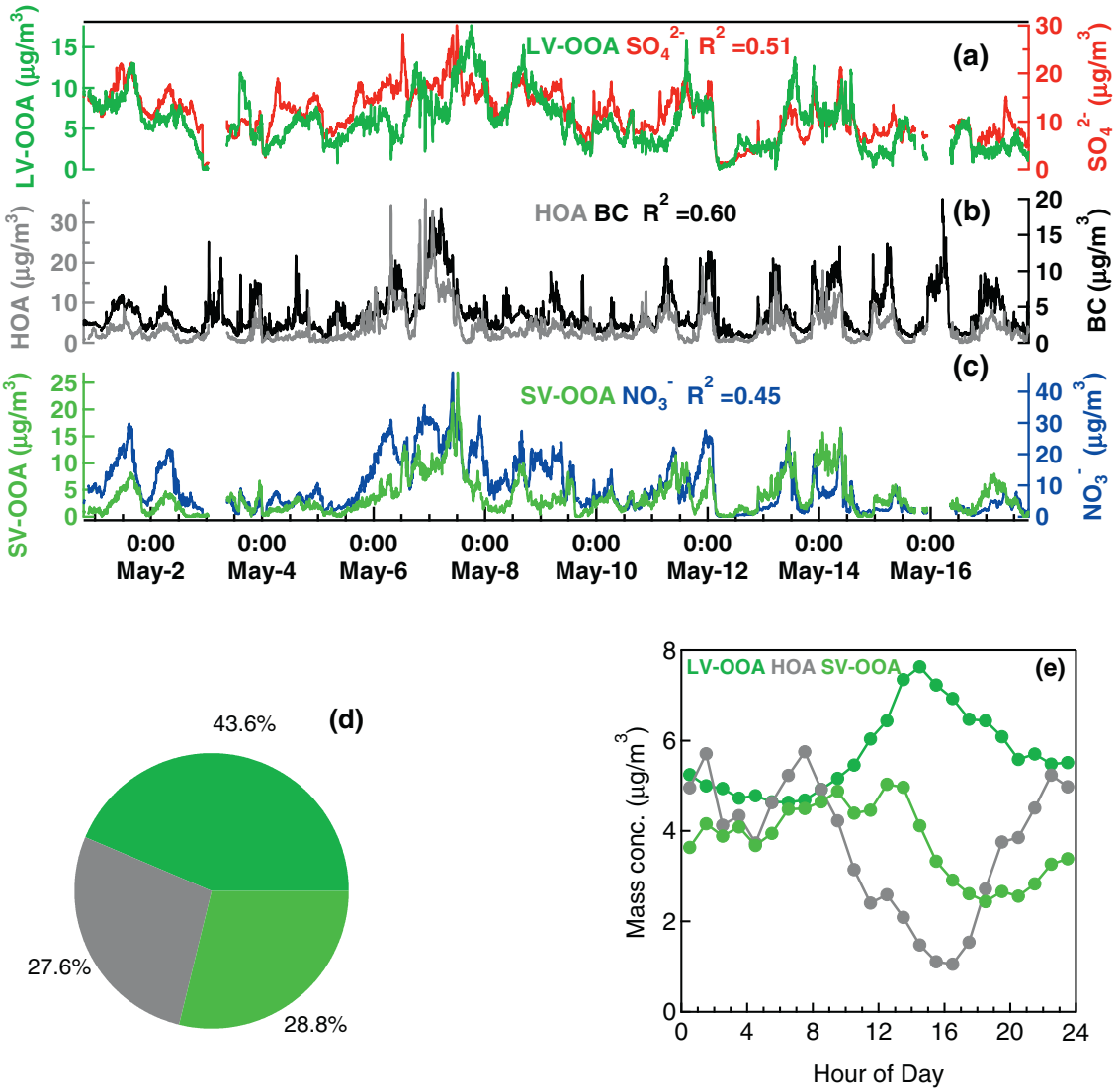

Fig. 5 – (a)–(c) Time series of the three organic components and the relevant species during the campaign; (d) the average constitution of the three components; (e) the diurnal variations of the three organic components in Xiamen.

(0.16 in A-A) (Aiken et al., 2009) and Beijing (0.17 in A-A) (Huang et al., 2010).

The MS of the two oxygenated organic aerosol, which were both characterized by prominent $C_xH_yO_z$ fragments, especially CO_2^+ (*m*/*z* 44) and $C_2H_3O^+$ (*m*/*z* 43), had O/C ratios of 0.48 for SV-OOA and 0.98 for LV-OOA in I-A method, respectively, indicating the presence of large amounts of oxidized organic compounds. The mass spectra showed different relative intensities of *m*/*z* 44, which can be used to classify these two OOA (Ng et al., 2010). SV-OOA, referred to semi-volatile oxygenated organic aerosol, is less oxidized and fresher than LV-OOA, which is referred to less-volatile oxygenated organic aerosol (Jimenez et al., 2009; Ng et al., 2010). The fraction of *m*/*z* 43 to organic mass (f43) is higher for SV-OOA and relatively lower for LV-OOA (Canonaco et al., 2015). With the elemental ratio calculated in A-A method, the O/C of SV-OOA and LV-OOA in Xiamen was 0.37 and 0.80, respectively. They are comparable to the O/C ratios reported by Ng et al. (2010): a wide range of O/C ratio for both LV-OOA (0.73 ± 0.14) and SV-OOA (0.35 ± 0.14) in A-A method. The two types of OOAs have been identified in many AMS aerosol datasets and shown to be a good surrogate of SOA (Zhang et al., 2005a, 2007; Jimenez et al., 2009; Ng et al., 2010). Due to the low volatility of LV-OOA and sulfate, semi-volatility of SV-OOA and nitrate, LV-OOA showed a better correlation with sulfate (R^2 = 0.51) rather than with nitrate (R^2 = 0.42) and SV-OOA correlated better with nitrate (R^2 = 0.45) rather than with sulfate (R^2 = 0.31), as what was shown in previous studies (Docherty et al., 2008; Huffman et al., 2009; Jimenez et al., 2009; Ng et al., 2010).

The diurnal patterns of the three organic components showed the time delay of the daytime peaks as reported previously (Jimenez et al., 2009; Huang et al., 2010). They showed the continuous chemical evolution of OA from HOA to SV-OOA, and then the oxidation from SV-OOA to LV-OOA, as OA was being oxidized in the atmosphere. The diurnal variation of HOA showed a daily peak at the early morning as HOA was emitted during early rush hour, and then decreasing at noon and increasing at night because of the volatility and the changing of planetary boundary layer height. As for the small peak of HOA at around 1:00 a.m., it

was very likely to be a result of more diesel vehicles running due to less traffic restriction at midnight. SV-OOA showed a peak after that of HOA due to the oxidation of HOA and VOCs and then decreasing because of the semi-volatile character and the lifting of the planetary boundary layer, while the diurnal variation of LV-OOA exhibited a later peak at about 14:00 as LV-OOA is expected to be formed by photochemical aging of SV-OOA and has less volatility (Fig. 5d). The increasing rate of LV-OOA was much larger than that of SV-OOA, suggesting that the evolution from SV-OOA to LV-OOA was much stronger than that from fresh local emissions of VOCs or HOA to SV-OOA. So it can be inferred that SOA in Xiamen was greatly influenced by regional aged air mass. OOA was considered as the sum of LV-OOA and SV-OOA, it showed a much better correlation with the sum of sulfate and nitrate (R^2 = 0.61), further confirming the characteristic of OOA as secondary organic aerosol.

2.6. Relationship of wind and submicron particles

The removal and transportation of submicron particles are deeply influenced by the wind direction and wind speed. TAQMN (Taiwan Air Quality Monitoring Network) showed the combination of long-range transport and local emission sources was an important reason for the accumulation of air pollutants in the offshore and coastal regions (Tsai et al., 2010).

Fig. 6 presents the mass concentration distribution of the chemical species related to the wind speed and wind direction in Xiamen. The major chemical species can be categorized into three similar pairs (LV-OOA and SO_4^{2-}, SV-OOA and NO_3^-, HOA and BC) by the mass concentration distribution with wind. All the species showed the highest mass concentration while the wind came from southeast with the wind speed between 1 and 3 m/s, indicating that there was important pollution input from the southeast. Since the remote area to the southeast of Xiamen is just the sea, the potential sources are inferred to be the local emissions in the southeast area of Xiamen. When there was a calm wind, BC and HOA also showed more frequent high mass concentrations, suggesting that fresh local emissions around the sampling site accumulated at this time. In comparison, SO_4^{2-} and LV-OOA showed a little more uniform distribution, consistent with the fact that they are more oxidized and aged species and are influenced more by regional transport through the Taiwan Strait. The distributions of SV-OOA and NO_3^- seemed to be a moderate case between those of the other two pairs.

3. Conclusions

Based on the Aerodyne HR-ToF-AMS measurement at a suburban site in Xiamen in May 2015, the chemical composition of the aerosols and source apportionment were obtained.

The mean PM_1 mass concentration was 46.2 ± 26.3 μg/m^3, ranged from 2.7 μg/m^3 to 164.4 μg/m^3 in 5 min time resolution. Organics, sulfate and nitrate were the most abundant species, accounted for 28.3%, 24.9% and 20.6%, respectively, followed by ammonium (16.2%), black carbon (8.9%) and chloride (1.1%). The percent of nitrate in total PM_1 mass increased the largest when PM_1 mass concentration increased, showing that NO_x emissions played a key role in high fine particle pollution in Xiamen. Evaluation of nitrate size distribution further indicated that local formation of nitrate on smaller particles are an important process for high nitrate pollution. In addition, the nitrate functionality from organic nitrates was found to account for 9.0–13.8% of the total nitrate.

PMF analysis results showed that OA can be divided into three subtypes, including primarily-emitted hydrocarbon-like OA (HOA), semi-volatile oxygenated OA (SV-OOA) and less-volatile oxygenated OA (LV-OOA). OOA totally accounted for

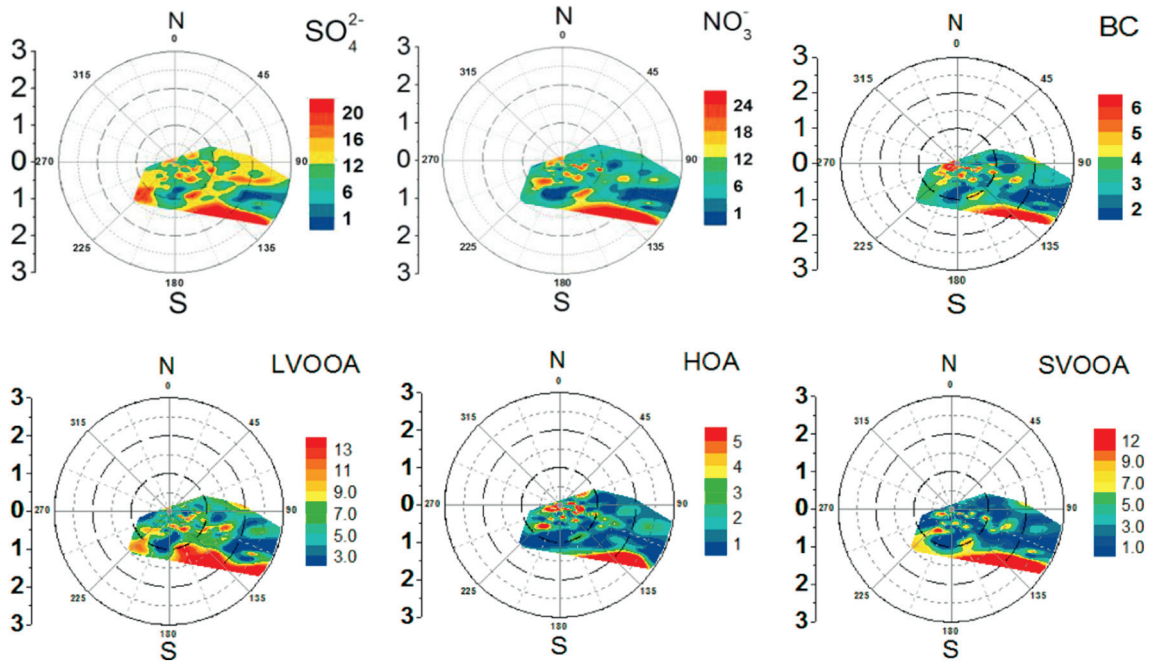

Fig. 6 – Distribution of the major submicron particle species with wind direction and speed in Xiamen.

about 72.4% (LV-OOA and SV-OOA accounted 43.6% and 28.8%, respectively) of OA, indicating that SOA dominated the OA in Xiamen and the sum of LV-OOA and SV-OOA showed high correlation with the sum of SO_4^{2-} and NO_3^-, verifying that they are formed by secondary reaction rather than being emitted directly. Generally, the strong evolution from SV-OOA to LV-OOA in the daytime suggested that SOA in Xiamen was greatly influenced by regional transport.

The correlation of the mass concentrations of major species with wind direction and wind speed revealed that they were all influenced by strong local sources in the southeast area of Xiamen, while SO_4^{2-} and LV-OOA were relatively more influenced by regional transport.

Acknowledgments

This work was supported by the National Natural Science Foundation of China (21277003), the Ministry of Science and Technology of China (2013CB228503), and the Shenzhen Science & Technology Plan.

REFERENCES

Aiken, A.C., DeCarlo, P.F., Jimenez, J.L., 2007. Elemental analysis of organic species with electron ionization high-resolution mass spectrometry. Anal. Chem. 79 (21), 8350–8358.

Aiken, A.C., Decarlo, P.F., Kroll, J.H., Worsnop, D.R., Huffman, J.A., Docherty, K.S., et al., 2008. O/C and OM/OC ratios of primary, secondary, and ambient organic aerosols with high-resolution time-of-flight aerosol mass spectrometry. Environ. Sci. Technol. 42 (12), 4478–4485.

Aiken, A.C., Salcedo, D., Cubison, M.J., Huffman, J.A., 2009. Mexico City aerosol analysis during MILAGRO using high resolution aerosol mass spectrometry at the urban supersite (T0) – part 1: fine particle composition and organic source apportionment. Atmos. Chem. Phys. 9 (17), 6633–6653.

Alfarra, M.R., Coe, H., Allan, J.D., Bower, K.N., Boudries, H., Canagaratna, M.R., et al., 2004. Characterization of urban and rural organic particulate in the lower Fraser Valley using two aerodyne aerosol mass spectrometers. Atmos. Environ. 38, 5745–5758.

Allan, J.D., Alfarra, M.R., Bower, K.N., Williams, P.I., Gallagher., M.W., Jimenez, J.L., et al., 2003. Quantitative sampling using an aerodyne aerosol mass spectrometer. Part 2: measurements of fine particulate chemical composition in two UK cities. J. Geophys. Res. Atmos. 108 (D9), 107–118.

Atkinson, R., 1997. Gas-phase tropospheric chemistry of volatile organic compounds: 1. Alkanes and alkenes. J. Phys. Chem. Ref. Data 26 (2), 215–290.

Atkinson, R., Arey, J., 2003. Atmospheric degradation of volatile organic compounds. Chem. Rev. 103 (12), 4605–4638.

Baklanov, A., Molina, L.T., Gauss, M., 2016. Megacities, air quality and climate. Atmos. Environ. 126, 235–249.

Boyd, C.M., Sanchez, J., Xu, L., Eugene, A.J., Nah, T., Tuet, W.Y., et al., 2015. Secondary organic aerosol formation from the β-pinene + NO3 system: effect of humidity and peroxy radical fate. Atmos. Chem. Phys. 15, 7497–7522.

Bruns, E.A., Perraud, V., Zelenyuk, A., Ezell, M.J., Johnson, S.N., Yu, Y., et al., 2010. Comparison of FTIR and particle mass spectrometry for the measurement of particulate organic nitrates. Environ. Sci. Technol. 44 (44), 1056–1061.

Canagaratna, M.R., Jayne, J.T., Ghertner, D.A., Herndon, S., Shi, Q., Jimenez, J.L., et al., 2004. Chase studies of particulate emissions from in-use New York City vehicles. Aerosol Sci. Technol. 38 (6), 555–573.

Canagaratna, M.R., Jayne, J.T., Jimenez, J.L., Allan, J.D., Alfarra, M.R., Zhang, Q., et al., 2007. Chemical and microphysical characterization of ambient aerosols with the aerodyne aerosol mass spectrometer. Mass Spectrom. Rev. 26 (2), 185–222.

Canagaratna, M.R., Jimenez, J.L., Kroll, J.H., Chen, Q., Kessler, S.H., Massoli, P., et al., 2015. Elemental ratio measurements of organic compounds using aerosol mass spectrometry: characterization, improved calibration, and implications. Atmos. Chem. Phys. 15, 253–272.

Canonaco, F., Slowik, J.G., Baltensperger, U., Prévôt, A.S.H., 2015. Seasonal differences in oxygenated organic aerosol composition: implications for emissions sources and factor analysis. Atmos. Chem. Phys. 15 (12), 6993–7002.

Day, D.A., Liu, S., Russell, L.M., Ziemann, P.J., 2010. Organonitrate group concentrations in submicron particles with high nitrate and organic fractions in coastal Southern California. Atmos. Environ. 44 (16), 1970–1979.

Decarlo, P.F., Kimmel, J.R., Trimborn, A., Northway, M.J., Jayne, J.T., Aiken, A.C., et al., 2006. Field-deployable, high-resolution, time-of-flight aerosol mass spectrometer. Anal. Chem. 78 (24), 8281–8289.

Deng, J., Xing, Z., Zhuang, B., Du, K., 2014. Comparative study on long-term visibility trend and its affecting factors on both sides of the Taiwan strait. Atmos. Res. 143 (12), 266–278.

Docherty, K.S., Stone, E.A., Ulbrich, I.M., DeCarlo, P.F., Snyder, D.C., Schauer, J.J., et al., 2008. Apportionment of primary and secondary organic aerosols in Southern California during the 2005 Study of Organic Aerosols in Riverside (SOAR-1). Environ. Sci. Technol. 42 (20), 7655–7662.

Drewnick, F., Hings, S.S., DeCarlo, P., Jayne, J.T., Gonin, M., Fuhrer, K., et al., 2005. A new time-of-flight aerosol mass spectrometer (TOF-AMS)-instrument description and first field deployment. Aerosol Sci. Technol. 39 (2005), 637–658.

Farmer, D.K., Matsunaga, A., Docherty, K.S., Surratt, J.D., Seinfeld, J.H., Ziemann, P.J., et al., 2010. Response of an aerosol mass spectrometer to organonitrates and organosulfates and implications for atmospheric chemistry. Proc. Natl. Acad. Sci. 107 (15), 6670–6675.

Feng, Y., Chen, Y., Guo, H., Zhi, G., Xiong, S., Li, J., et al., 2009. Characteristics of organic and elemental carbon in $PM_{2.5}$, samples in Shanghai, China. Atmos. Res. 92 (4), 434–442.

Fry, J.L., Kiendlerscharr, A., Rollins, A.W., Wooldridge, P.J., Brown, S.S., Fuchs, H., et al., 2009. Organic nitrate and secondary organic aerosol yield from NO_3 oxidation of β-pinene evaluated using a gas-phase kinetics/aerosol partitioning model. Atmos. Chem. Phys. 9 (3), 1431–1449.

Gong, H.M., Matsunaga, A., Ziemann, P.J., 2005. Products and mechanism of secondary organic aerosol formation from reactions of linear alkenes with NO_3 radicals. J. Phys. Chem. A 109 (19), 4312–4324.

He, L.-Y., Huang, X.-F., Xue, L., Hu, M., Lin, Y., Zheng, J., et al., 2011. Submicron aerosol analysis and organic source apportionment in an urban atmosphere in Pearl River Delta of China using high-resolution aerosol mass spectrometry. J. Geophys. Res.: Atmos. 116 (D12), 1248–1256.

Hennigan, C.J., Sullivan, A.P., Fountoukis, C.I., Nenes, A., Hecobian, A., Vargas, O., et al., 2008. On the volatility and production mechanisms of newly formed nitrate and water soluble organic aerosol in Mexico City. Atmos. Chem. Phys. 8, 4811–4829.

Hu, W., Hu, M., Hu, W., Jimenez, J.L., Yuan, B., Chen, W., et al., 2016. Chemical composition, sources, and aging process of submicron aerosols in Beijing: contrast between summer and winter. J. Geophys. Res. Atmos. 121 (4), 1955–1977.

Huang, X.F., He, L.Y., Hu, M., Canagaratna, M.R., Sun, Y., Zhang, Q., et al., 2010. Highly time-resolved chemical characterization of atmospheric submicron particles during 2008 Beijing Olympic

games using an aerodyne high-resolution aerosol mass spectrometer. Atmos. Chem. Phys. 10 (18), 8933–8945.
Huang, X.F., He, L.Y., Xue, L., Sun, T.L., Zeng, L.W., Gong, Z.H., et al., 2012. Highly time-resolved chemical characterization of atmospheric fine particles during 2010 Shanghai world expo. Atmos. Chem. Phys. 12 (11), 4897–4907.
Huang, X.F., Xue, L., Tian, X.D., Shao, W.W., Sun, T.L., Gong, Z.H., et al., 2013. Highly time-resolved carbonaceous aerosol characterization in Yangtze River Delta of China: composition, mixing state and secondary formation. Atmos. Environ. 64, 200–207.
Huang, R.J., Zhang, Y., Bozzetti, C., Ho, K.F., Cao, J.J., Han, Y., et al., 2014. High secondary aerosol contribution to particulate pollution during haze events in China. Nature 514 (7521), 218–222.
Huffman, J.A., Docherty, K.S., Aiken, A.C., Cubison, M.J., Ulbrich, I.M., Decarlo, P.F., et al., 2009. Chemically-resolved aerosol volatility measurements from two megacity field studies. Atmos. Chem. Phys. 9 (18), 7161–7182.
IPCC, 2013. IPCC Fifth Assessment Report: the Physical Science Basis, Working Group I, Final Report, Geneva, Switzerland.
Jayne, J.T., Leard, D.C., Zhang, X.F., Davidovits, P., Smith, K.A., Kolb, C.E., et al., 2000. Development of an aerosol mass spectrometer for size and composition analysis of submicron particles. Aerosol Sci. Technol. 33 (1), 49–70.
Jimenez, J.L., Jayne, J.T., Shi, Q., Kolb, C.E., Worsnop, D.R., Yourshaw, I., et al., 2003. Ambient aerosol sampling using the aerodyne aerosol mass spectrometer. J. Geophys. Res. Atmos. 108 (8425), 447–457.
Jimenez, J.L., Canagaratna, M.R., Donahue, N.M., Prevot, A.S., Zhang, Q., Kroll, J.H., et al., 2009. Evolution of organic aerosols in the atmosphere. Science 326 (5959), 1525–1529.
Lanz, V.A., Alfarra, M.R., Baltensperger, U., Buchmann, B., Hueglin, C., Prvt, A.S.H., 2007. Source apportionment of submicron organic aerosols at an urban site by factor analytical modelling of aerosol mass spectra. Atmos. Chem. Phys. 7 (6), 1503–1522.
Laurent, J.P., Allen, D.T., 2004. Size distributions of organic functional groups in ambient aerosol collected in Houston, Texas. Aerosol Sci. Technol. 38 (1), 82–91.
Lim, Y.B., Ziemann, P., 2009. Chemistry of secondary organic aerosol formation from OH radical-initiated reactions of linear, branched, and cyclic alkanes in the presence of NO_x. Aerosol Sci. Technol. 34 (43), 604–619.
Matsunaga, A., Ziemann, P.J., 2009. Yields of beta-hydroxynitrates and dihydroxynitrates in aerosol formed from OH radical-initiated reactions of linear alkenes in the presence of $NO_{(x)}$. J. Appl. Polym. Sci. 113 (3), 599–606.
Matthew, B.M., Middlebrook, A.M., Onasch, T.B., 2008. Collection efficiencies in an aerodyne aerosol mass spectrometer as a function of particle phase for laboratory generated aerosols. Aerosol Sci. Technol. 42 (42), 884–898.
Middlebrook, A.M., Bahreini, R., Jimenez, J.L., Canagaratna, M.R., 2012. Evaluation of composition-dependent collection efficiencies for the aerodyne aerosol mass spectrometer using field data. Aerosol Sci. Technol. 46 (3), 258–271.
Mohr, C., Huffman, A., Cubison, M.J., Aiken, A.C., Docherty, K.S., Kimmel, J.R., et al., 2009. Characterization of primary organic aerosol emissions from meat cooking, trash burning, and motor vehicles with high-resolution aerosol mass spectrometry and comparison with ambient and chamber observations. Environ. Sci. Technol. 43 (7), 2443–2449.
Mylonas, D.T., Allen, D.T., Ehrman, S.H., Pratsinis, S.E., 1991. The sources and size distributions of organonitrates in Los-Angeles aerosol. Atmos. Environ. Part A Gen. Top. 25 (12), 2855–2861.
Ng, N.L., Kwan, A.J., Surratt, J.D., Chan, A.W.H., Chhabra, P.S., Sorooshian, A., et al., 2008. Secondary organic aerosol (SOA) formation from reaction of isoprene with nitrate radicals(NO_3). Atmos. Chem. Phys. 8, 4117–4140.
Ng, N.L., Canagaratna, M.R., Zhang, Q., Jimenez, J.L., Tian, J., Ulbrich, I.M., et al., 2010. Organic aerosol components observed in northern hemispheric datasets from aerosol mass spectrometry. Atmos. Chem. Phys. 10 (10), 4625–4641.
O'Brien, R.J., Crabtree, J.H., Holmes, J.R., Hoggan, M.C., Bockian, A.H., 1975. Formation of photochemical aerosol from hydrocarbons. Atmospheric analysis. Environ. Sci. Technol. 9 (6), 577–582.
Paatero, P., Hopke, P.K., 2003. Discarding or downweighting high-noise variables in factor analytic models. Anal. Chim. Acta 490 (1), 277–289.
Paatero, P., Tapper, U., 1994. Positive matrix factorization–a nonnegative factor model with optimal utilization of error-estimates of data values. Environmetrics 5 (2), 111–126.
Roberts, J.M., 1990. The atmospheric chemistry of organic nitrates. Atmos. Environ. Part A Gen. Top. 24 (2), 243–287.
Rollins, A.W., Fry, J.L., Hunter, J.F., Kroll, J.H., Worsnop, D.R., Singaram, S.W., et al., 2010. Elemental analysis of aerosol organic nitrates with electron ionization high-resolution mass spectrometry. Atmos. Meas. Tech. 3, 301–310.
Salcedo, D., Onasch, T.B., Dzepina, K., Canagaratna, M.R., Zhang, Q., Huffman, J.A., et al., 2006. Characterization of ambient aerosols in Mexico City during the MCMA-2003 campaign with aerosol mass spectrometry: results from the CENICA supersite. Atmos. Chem. Phys. 6 (4), 925–946.
Sato, K., Takami, A., Isozaki, T., Hikida, T., Shimono, A., 2010. Mass spectrometric study of secondary organic aerosol formed from the photo-oxidation of aromatic hydrocarbons. Atmos. Environ. 44, 1080–1087.
Sun, Y., Zhang, Q., Macdonald, A.M., Hayden, K., 2009. Size-resolved aerosol chemistry on Whistler Mountain, Canada with a high-resolution aerosol mass spectrometer during Intex-B. Atmos. Chem. Phys. 9 (9), 3095–3111.
Tsai, H.H., Yuan, C.S., Hung, C.H., Lin, Y.C., 2010. Comparing physicochemical properties of ambient particulate matter of hot spots in a highly polluted air quality zone. Aerosol Air Qual. Res 10 (4), 331–344.
Ulbrich, I.M., Canagaratna, M.R., Zhang, Q., Worsnop, D.R., 2009. Interpretation of organic components from positive matrix factorization of aerosol mass spectrometric data. Atmos. Chem. Phys. 8 (2), 2891–2918.
Wu, S.P., 2015. Two-years $PM_{2.5}$ observations at four urban sites along the coast of southeastern China. Aerosol Air Qual. Res. 15.
Xiao, R., Takegawa, N., Kondo, Y., Miyazaki, Y., Miyakawa, T., Hu, M., et al., 2009. Formation of submicron sulfate and organic aerosols in the outflow from the urban region of the pearl river delta in China. Atmos. Environ. 43 (24), 3754–3763.
Xu, L., Suresh, S., Guo, H., Weber, R.J., Ng, N.L., 2015. Aerosol characterization over the southeastern United States using high-resolution aerosol mass spectrometry: spatial and seasonal variation of aerosol composition and sources with a focus on organic nitrates. Atmos. Chem. Phys. 15, 7307–7336.
Yan, J., Chen, L., Lin, Q., Li, Z., Chen, H., Zhao, S., 2015. Chemical characteristics of submicron aerosol particles during a long-lasting haze episode in Xiamen, China. Atmos. Environ. 113, 118–126.
Zhang, Q., Canagaratna, M.R., Jayne, J.T., Worsnop, D.R., Jimenez, J., 2005a. Time-and size-resolved chemical composition of submicron particles in Pittsburgh: implications for aerosol sources and processes. J. Geophys. Res. Atmos. 110 (7), 191–206.
Zhang, Q., Worsnop, D.R., Canagaratna, M.R., Jimenez, J.L., 2005b. Hydrocarbon-like and oxygenated organic aerosols in Pittsburgh: insights into sources and processes of organic aerosols. Atmos. Chem. Phys. 5 (Suppl. 1), 3289–3311.
Zhang, Q., Jimenez, J.L., Canagaratna, M.R., Allan, J.D., Coe, H., Ulbrich, I., 2007. Ubiquity and dominance of oxygenated species in organic aerosols in anthropogenically-influenced northern hemisphere Midlatitudes. Geophys. Res. Lett. 34, L13801.
Zhang, F., Xu, L., Chen, J., Yu, Y., Niu, Z., Yin, L., 2012. Chemical compositions and extinction coefficients of PM2.5, in

peri-urban of Xiamen, China, during June 2009–May 2010. Atmos. Res. 106 (106), 150–158.

Zhang, F., Chen, J., Qiu, T., Yin, L., Chen, X., Yu, J., 2013. Pollution characteristics of $PM_{2.5}$ during a typical haze episode in Xiamen, China. Atmos. Clim. Sci. 3 (4), 427–439.

Zheng, J., Zhang, R., Fortner, E.C., Volkamer, R.M., 2008. Measurements of HNO3 and N2O5 using ion drift-chemical ionization mass spectrometry during the MILAGRO/MCMA-2006 campaign. Atmos. Chem. Phys. 8 (22), 6823–6838.